

Geminin deficiency enhances survival in a murine medulloblastoma model by inducing apoptosis of preneoplastic granule neuron precursors – Sankar etal

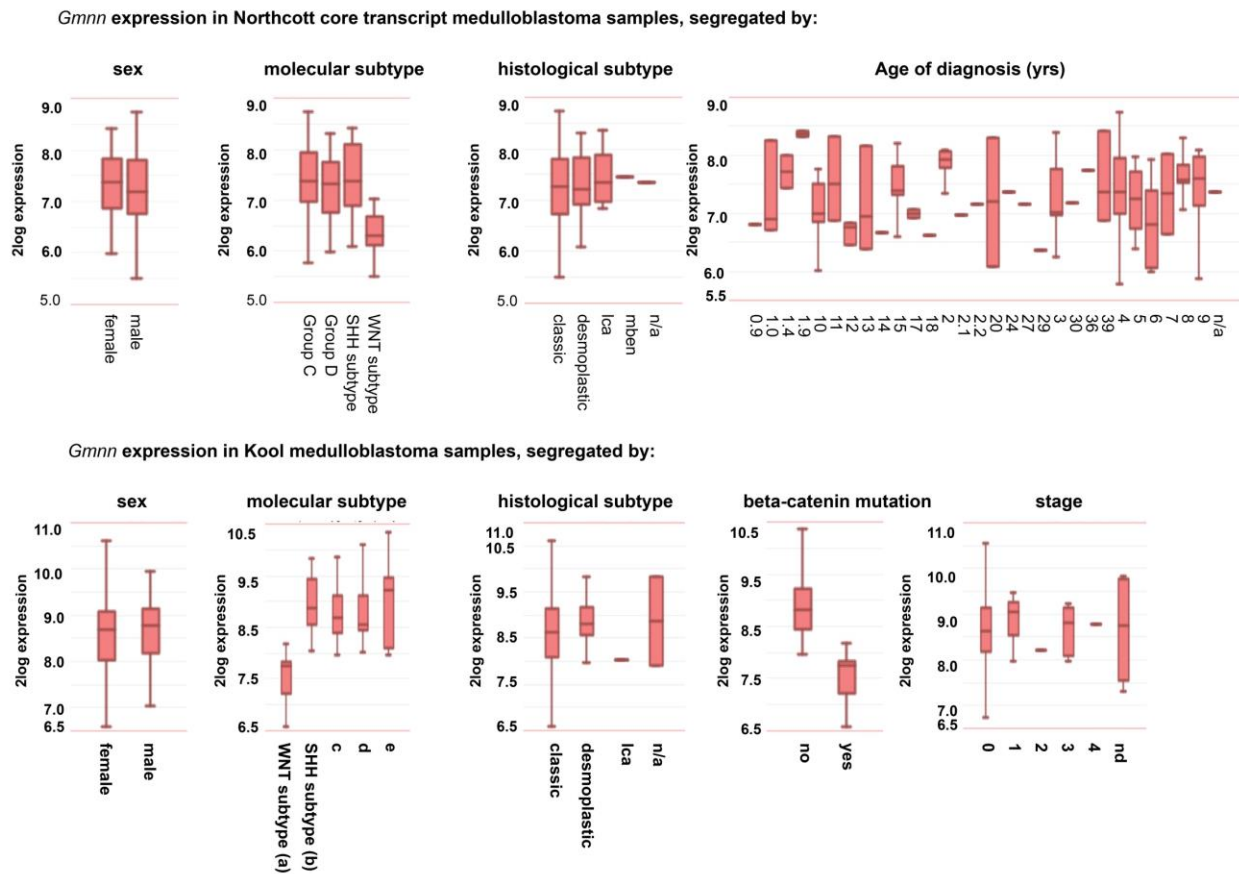


Figure S1: Geminin expression levels in medulloblastomas do not correlate with tumor molecular or histological subtypes, staging, age of diagnosis, or sex. Geminin expression levels were analyzed in two human medulloblastoma datasets by using the R2 Megasampler tool (see Methods; datasets used were Northcott core transcript, n=103, GSE21140 and Kool, n=62, GSE10327) and did not segregate based upon sex, molecular or histological subtype, age of diagnosis, or stage. *Gmnn* is on human chr6 and expression levels are lower in the Wnt and β -catenin mutated subtypes, congruent with monosomy 6 in the Wnt tumor subclass.

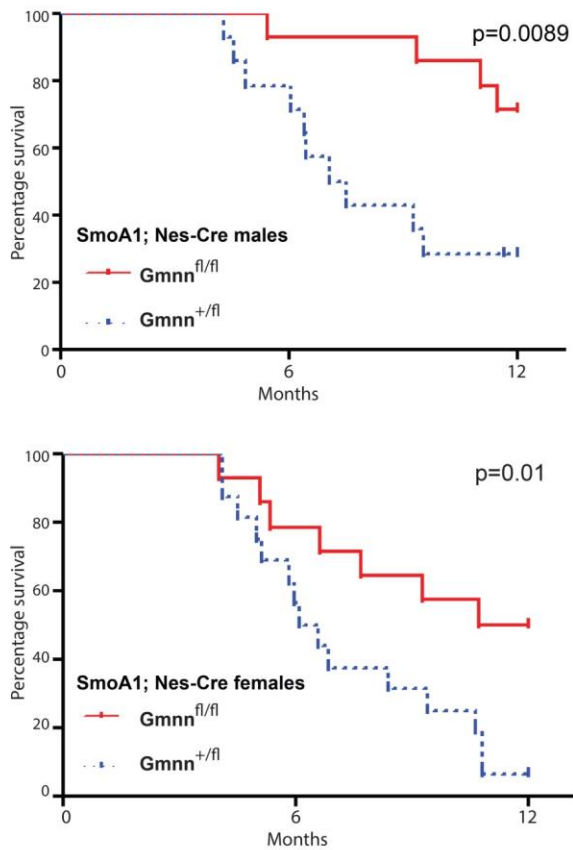


Figure S2: Geminin loss of function enhances survival in the SmoA1 medulloblastoma model.

Kaplan-Meier survival plot is shown for cohorts of male or female mice hemizygous for both the Nes-Cre and SmoA1 transgenes and either heterozygous or homozygous for the floxed Gem allele. Animals were euthanized by transcardial perfusion when they exhibited neurologic impairment or morbidity or at the end of the study and presence or absence of tumors assessed by sectioning and histology.

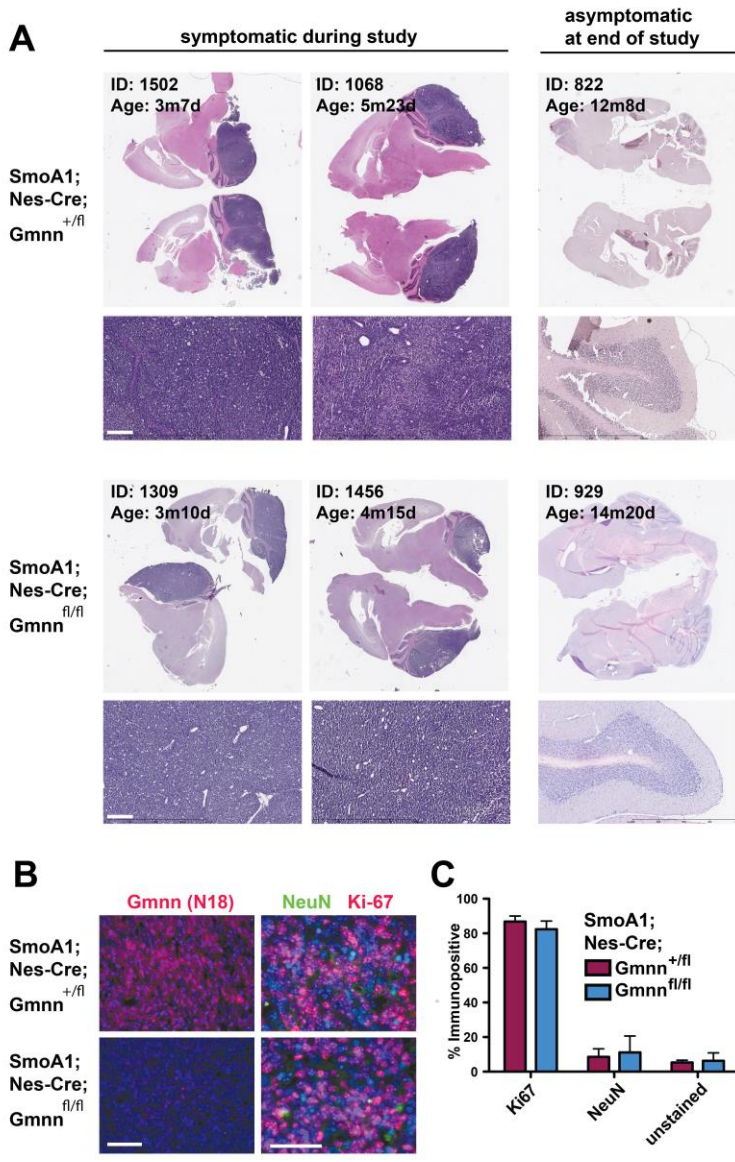


Figure S3: Histology and molecular marker expression in SmoA1 tumors. (A) Cohorts of mice with the SmoA1; Nes-Cre; Gmnn^{+/-fl} and SmoA1; Nes-Cre; Gmnn^{fl/fl} genotypes were generated and tracked for one year. Mice that developed clinical symptoms of medulloblastoma (enlarged posterior fossa, tilted head, hunched posture, ataxia) and animals that remained asymptomatic through the end of the study were euthanized and histological sectioning of the brain was performed. Examples are shown, with identification number and age at the time euthanized indicated. Parasagittal sections of all symptomatic animals revealed large, bilateral tumor masses, while very few animals that remained asymptomatic

through the end of the study exhibited a visible tumor mass. Lower panels: higher magnification views through the tumor or cerebellum. Tumor size and histology appeared similar between the two genotypes. Scale bar=200 μ m. **(B)** For each genotype, three tumors were also analyzed by frozen sectioning and immunofluorescence for Gmnn, Ki67, and NeuN, with DAPI (blue) counterstaining of all nuclei. Scale bars=50 μ m, with **(C)** numbers of Ki67 or NeuN immunopositive cells scored for three sections through each tumor and expressed as a percentage +/- stdev. Gmnn protein levels were strongly diminished in the SmoA1; Nes-Cre; Gmnn^{fl/fl} tumors, while similar fractions of cells expressing Ki67 or NeuN were seen for both genotypes.

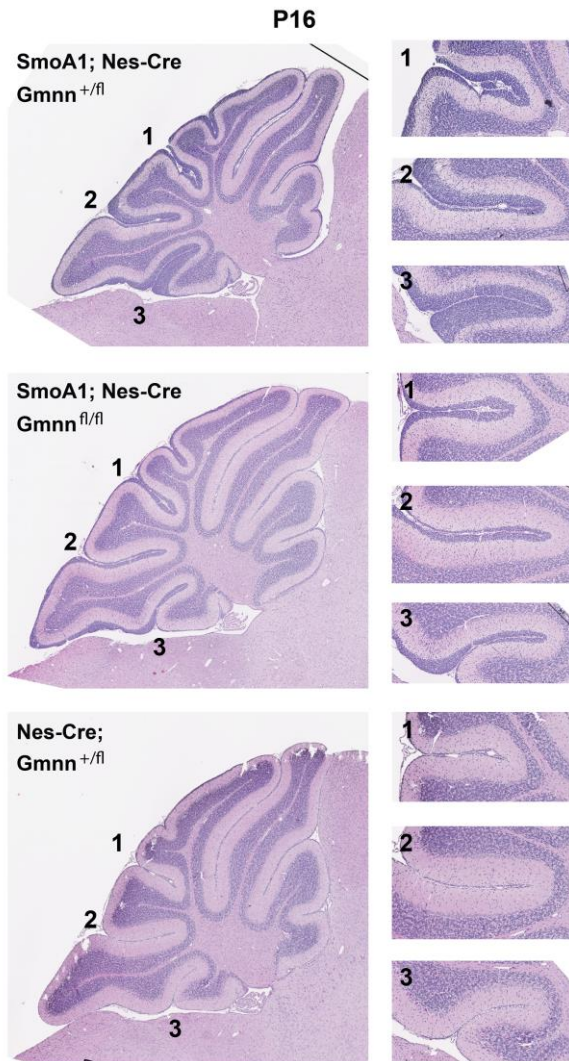


Figure S4: Geminin loss reduces numbers of persisting preneoplastic GNPs in SmoA1 mice.

Animals hemizygous for the SmoA1 and Nes-Cre transgenes and heterozygous for the Gmnn floxed allele (SmoA1; Nes-Cre; Gmnn^{+/fl}) retained much thicker EGL regions in P16 cerebellar sections than those seen in SmoA1; Nes-Cre; Gmnn^{fl/fl} homozygous animals, with animals lacking the SmoA1 transgene shown as an additional control.

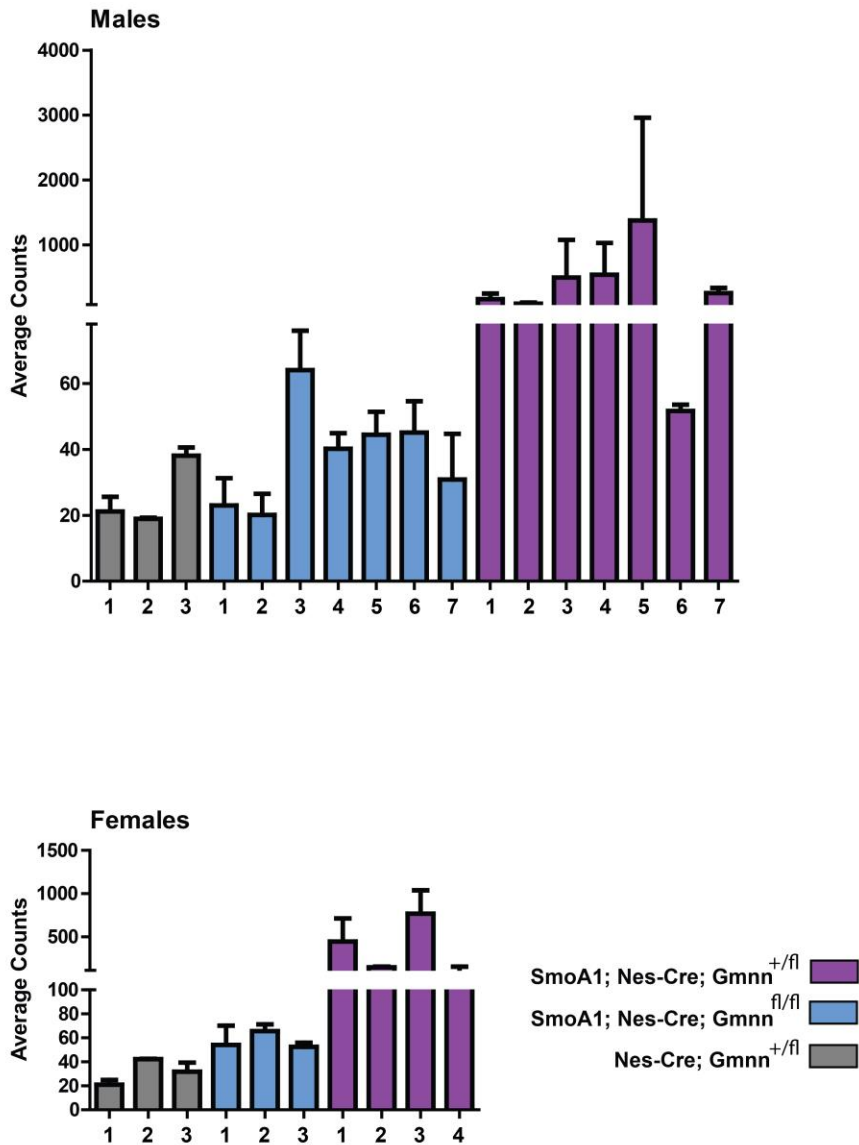


Figure S5: Quantitation of GNPs at the cerebellar surface in individual P28 animals, comparing animals hemizygous for the SmoA1 and Nes-Cre transgenes and heterozygous versus homozygous for the Gmnn floxed allele, with animals lacking the SmoA1 transgene as an additional control.

Quantitative data (summarized for all animals in **Fig. 3D**) was obtained as averaged counts/section from 4 matched serial sections per brain, and is shown as averaged counts for each animal assayed. SmoA1; Nes-Cre; Gmnn^{fl/fl} homozygous P28 animals had six-fold fewer pGNPs than SmoA1; Nes-Cre; Gmnn^{+/fl} heterozygotes.

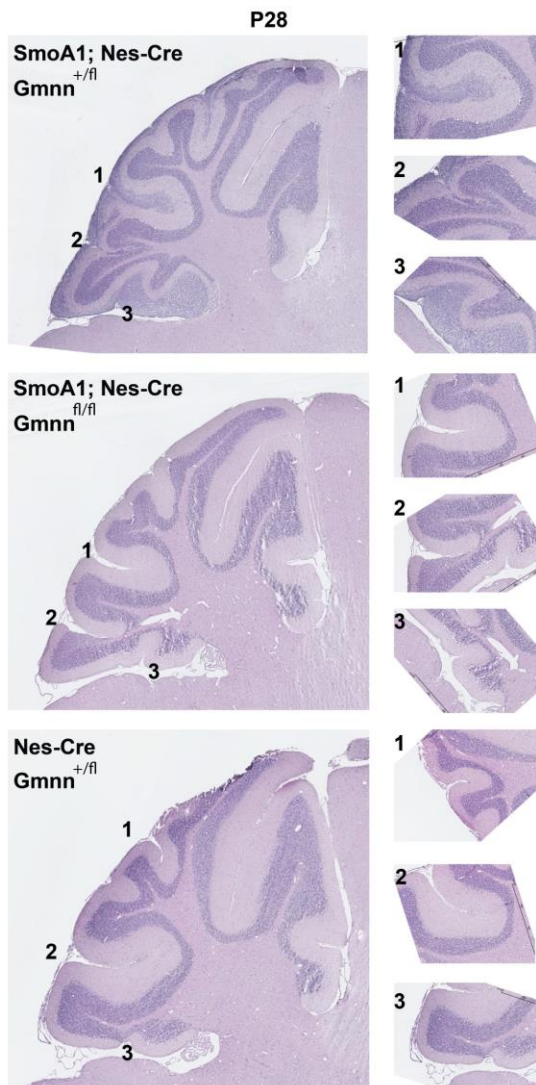


Figure S6: Example of severe dysplasia seen in some P28 animals hemizygous for the Nes-Cre and SmoA1 transgenes and heterozygous for the floxed Gmnn allele. This was not observed in any of the Nes-Cre; SmoA1 animals homozygous for the floxed Gmnn allele. Example of one representative animal for each genotype is shown.

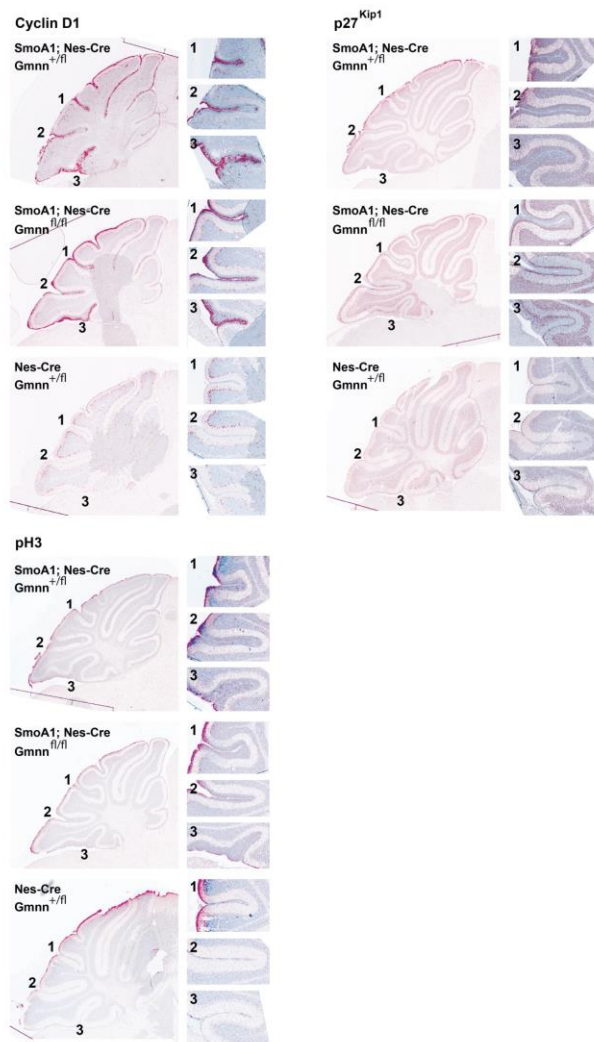


Figure S7: Immunohistochemistry for Cyclin D1, p27^{Kip1}, and pH3 on P14 cerebellar sections from animals hemizygous for the Nes-Cre and SmoA1 transgenes and either heterozygous or homozygous for the Gmnn floxed allele. No significant differences in the relative frequency of GNPs immunopositive for these antibodies was observed between animals heterozygous versus homozygous for the Gmnn floxed allele.

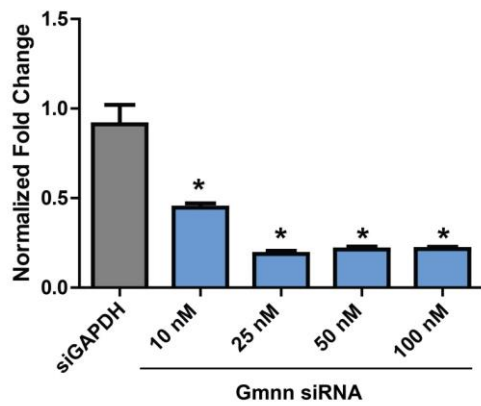


Figure S8: Gmnn siRNA dose response in Daoy cells. Daoy cells were transfected with increasing concentrations of a Gmnn siRNA (#2) as shown. After 72 hrs., Gmnn mRNA levels were analyzed by qRT-PCR, represented as normalized fold change relative to the control (siGAPDH). Subsequent experiments used the lowest dose of Gmnn siRNA #2 that provided effective knockdown (25 nM).

* <0.05 was defined by two-tailed student's t-test.

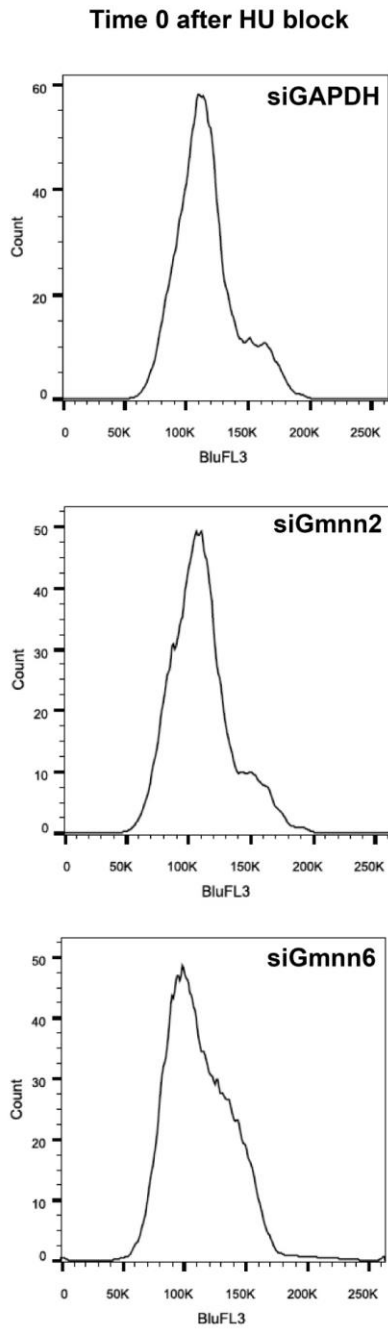


Figure S9: Cell cycle synchronization of Daoy cells. Synchronization with 100 nM hydroxyurea (HU) was performed for 14 hrs as described (see Methods). Time 0 after release from HU was analyzed by flow cytometry analysis with PI stained cells. In all three knockdown conditions, cells are predominantly synchronized in G1/S of cell cycle.

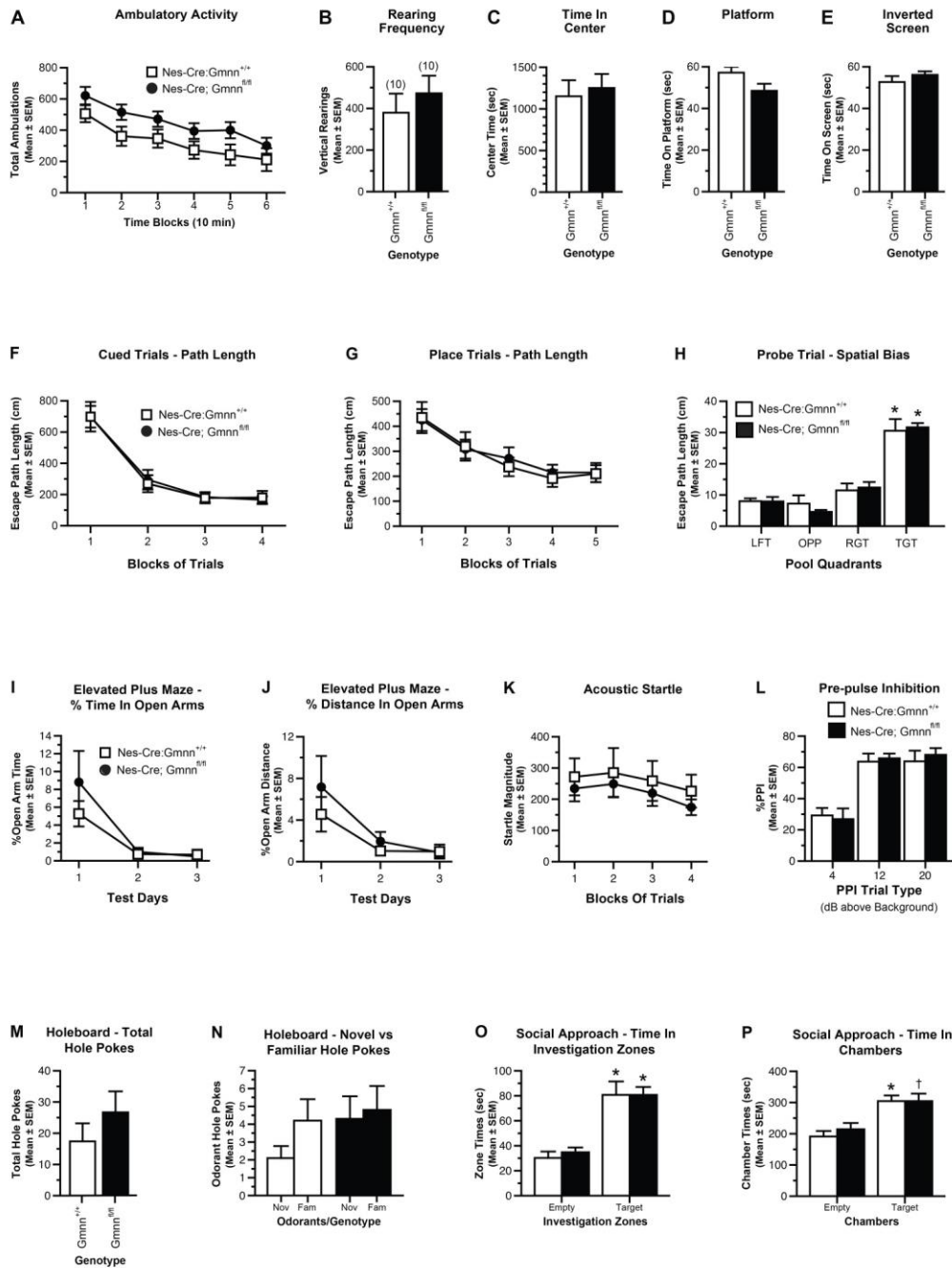


Figure S10: Behavioral testing failed to reveal a definitive phenotype in Nes-Cre; Gmnn conditional loss of function mice. To characterize any behavioral phenotypes resulting from Nes-Cre-mediated Geminin conditional loss of function, we generated cohorts of 3-4 month old mice that were hemizygous for the Nes-Cre transgene and either wild-type for Gmnn (Nes-Cre; Gmnn^{+/+}; n=10;

males=5/females=5) or homozygous for the floxed *Gmnn* allele (Nes-Cre; *Gmnn*^{fl/fl})(n=10; males=5/females=5). These were evaluated utilizing a range of behavioral analyses, as described in the Supplemental Methods and Results. **(A-C)** Results from a 1-h locomotor activity test showed that the *Gmnn*^{+/+} and *Gmnn*^{fl/fl} groups did not differ in terms of ambulatory activity **(A)**, vertical rearing frequency **(B)** or in time spent in the center of the test field **(C)**. **(D-E)** The *Gmnn*^{+/+} and *Gmnn*^{fl/fl} mice also did not differ significantly on the platform **(D)** or inverted screen **(E)** tests, which were part of the battery of sensorimotor measures. **(F-H)** Testing in the Morris water maze did not reveal any cognitive deficits in the *Gmnn*^{+/+} and *Gmnn*^{fl/fl} mice in terms of acquisition performance during the cued **(F)** or place (spatial) learning **(G)** trials. Likewise, the groups both showed intact retention during the probe trial by exhibiting a spatial bias for the target quadrant that had contained the submerged platform **(H)**. This was documented by each group spending significantly more time in the target quadrant versus the times spent in each of the other quadrants (*p<0.008). **(I-J)** Elevated plus maze test assessed time spent and distance travelled in the open arms relative to total time/distance in all of the arms and did not detect significant differences. **(K-L)** Analysis of the acoustic startle/PPI data indicated that the groups did not differ in terms of the magnitude of the ASR **(K)**, nor in %PPI levels **(L)**, suggesting that sensorimotor reactivity and gating did not differ in the *Gmnn*^{+/+} and *Gmnn*^{fl/fl} mice. **(M-N)** Analysis of the data from the holeboard exploration/olfactory preference test showed that the *Gmnn*^{+/+} and *Gmnn*^{fl/fl} groups did not differ in terms of total exploratory hole pokes **(M)** or in terms of poke frequencies for corner holes that contained a novel versus a familiar odorant **(N)**. **(O-P)** The results from the social approach test did not provide evidence of abnormal behaviors on the part of the *Gmnn*^{fl/fl} mice. Specifically, the *Gmnn*^{+/+} and *Gmnn*^{fl/fl} groups showed similar degrees of sociability by exhibiting significantly increased investigation zone times surrounding the stimulus mouse **(O)** relative to the times in the zones around the empty withholding cage (*p<0.00005), and each group spent more time in the chamber containing the stimulus mouse **(P)** compared to the empty chamber (*p=0.003; †p=0.035).

Tables S1-S3: Genes whose expression is most strongly correlated with that of Geminin in 103 medulloblastoma samples were defined for the Northcott core transcript dataset (GSE21140) using the R2 Megasampler (<http://hgserver1.amc.nl/cgi-bin/r2/main.cgi>). GO terms for genes with Gmnn co-correlated (**Table S1**) and anti-correlated (**Table S2**) expression and genes with Gmnn co-correlated expression (**Table S3**) are shown.

Geminin expression co-correlated GO terms

Enrichment by Process Networks			
#	Networks	p-value	FDR
1	Cell cycle_Core	1.37E-15	5.60E-14
2	Cell cycle_Mitosis	1.08E-12	2.21E-11
3	Cytoskeleton_Spindle microtubules	1.07E-11	1.47E-10
4	Cell cycle_S phase	2.65E-11	2.72E-10
5	Cell cycle_G2-M	1.81E-08	1.48E-07
6	DNA damage_MMR repair	6.26E-05	4.28E-04
7	Transcription_mRNA processing	1.00E-03	5.86E-03
8	DNA damage_DBS repair	1.47E-03	7.52E-03
9	Cell cycle_Meiosis	7.19E-03	3.28E-02
10	Transcription_Chromatin modification	1.37E-02	5.15E-02

Enrichment by GO Molecular Functions			
#	Molecular functions	p-value	FDR
1	nucleotide binding	2.47E-07	1.57E-05
2	protein binding	3.31E-07	1.57E-05
3	ATP binding	3.32E-07	1.57E-05
4	protein serine/threonine kinase activity	6.09E-07	2.16E-05
5	damaged DNA binding	2.01E-06	5.70E-05
6	transferase activity, transferring phosphorus-containing groups	4.94E-05	1.17E-03
7	DNA binding	7.62E-05	1.54E-03
8	kinetochore binding	8.73E-05	1.55E-03
9	kinase activity	1.05E-04	1.66E-03
10	single-stranded DNA binding	2.32E-04	3.30E-03

Enrichment by GO Processes			
#	Processes	p-value	FDR
1	cell cycle	1.20E-29	5.48E-27
2	mitotic cell cycle	9.85E-25	2.26E-22
3	cell division	3.02E-18	4.61E-16
4	mitosis	1.29E-17	1.48E-15
5	chromosome segregation	6.43E-11	5.89E-09
6	nucleosome assembly	1.59E-09	1.22E-07
7	response to DNA damage stimulus	4.78E-09	3.13E-07
8	DNA repair	1.19E-08	6.80E-07
9	G1/S transition of mitotic cell cycle	2.03E-08	1.03E-06
10	attachment of spindle microtubules to kinetochore	2.66E-08	1.22E-06

Enrichment by Pathway Maps			
#	Maps	p-value	FDR
1	Cell cycle_Role of APC in cell cycle regulation	2.59E-11	1.14E-09
2	Cell cycle_The metaphase checkpoint	6.36E-11	1.40E-09
3	Cell cycle_Start of DNA replication in early S phase	1.38E-07	2.02E-06
4	Cell cycle_Chromosome condensation in prometaphase	1.20E-06	1.32E-05
5	Cell cycle_Role of Nek in cell cycle regulation	6.98E-06	5.81E-05
6	Cell cycle_Spindle assembly and chromosome separation	7.92E-06	5.81E-05
7	DNA damage_Mismatch repair	6.29E-05	3.95E-04
8	Reproduction_Progesterone-mediated oocyte maturation	5.16E-04	2.84E-03
9	Cell cycle_Initiation of mitosis	4.37E-03	2.08E-02
10	DNA damage_ATM / ATR regulation of G2 / M checkpoint	4.72E-03	2.08E-02

Enrichment by GO Localizations			
#	Localizations	p-value	FDR
1	nucleus	9.71E-22	1.02E-19
2	condensed chromosome kinetochore	2.27E-16	1.19E-14
3	nucleoplasm	4.78E-15	1.67E-13
4	chromosome, centromeric region	6.69E-14	1.69E-12
5	chromosome	8.06E-14	1.69E-12
6	kinetochore	1.65E-13	2.89E-12
7	cytosol	5.19E-08	7.78E-07
8	spindle	1.72E-07	2.26E-06
9	condensed chromosome, centromeric region	4.72E-07	5.50E-06
10	centrosome	1.36E-06	1.43E-05

Geminin expression anti-correlated GO terms

#	Networks	p-value	FDR
1	Transport_Calcium transport	2.363E-02	6.633E-01
2	Neurophysiological process_Transmission of nerve impulse	3.247E-02	6.633E-01
3	Transport_Sodium transport	4.133E-02	6.633E-01
4	Reproduction_Male sex differentiation	5.145E-02	6.633E-01
5	Signal transduction_Neuropeptide signaling pathways	5.871E-02	6.633E-01
6	Muscle contraction	7.628E-02	6.633E-01
7	Inflammation_Innate inflammatory response	8.476E-02	6.633E-01
8	Cell adhesion_Synaptic contact	8.804E-02	6.633E-01
9	Neurophysiological process_Olfactory transduction	1.038E-01	6.633E-01
10	Reproduction_Gonadotropin regulation	1.052E-01	6.633E-01
Enrichment by GO Molecular Functions			
#	Molecular functions	p-value	FDR
1	enzyme activator activity	2.048E-10	3.626E-08
2	lipid binding	2.676E-05	2.368E-03
3	ion channel activity	2.752E-04	1.623E-02
4	voltage-gated calcium channel activity	4.805E-04	2.111E-02
5	high voltage-gated calcium channel activity	6.702E-04	2.111E-02
6	calcium channel activity	7.156E-04	2.111E-02
7	protein-hormone receptor activity	8.353E-04	2.112E-02
8	5-hydroxy-6E,8Z,11Z,14Z-icosatetraenoic acid binding	4.385E-03	4.085E-02
9	somatostatin receptor binding	4.385E-03	4.085E-02
10	fucokinase activity	4.385E-03	4.085E-02
Enrichment by GO Processes			
#	Processes	p-value	FDR
1	positive regulation of peptide secretion	2.740E-07	1.982E-04
2	negative regulation of heart rate	3.621E-07	1.982E-04
3	cytoskeletal anchoring at plasma membrane	8.041E-07	2.201E-04
4	negative regulation of hormone secretion	8.041E-07	2.201E-04
5	smooth muscle contraction involved in micturition	2.376E-06	5.203E-04
6	regulation of vasodilation	3.251E-06	5.490E-04
7	adult walking behavior	3.510E-06	5.490E-04
8	transmission of nerve impulse	5.213E-06	6.601E-04
9	negative regulation of renal sodium excretion	5.668E-06	6.601E-04
10	calcium ion import	6.028E-06	6.601E-04
Enrichment by Pathway Maps			
#	Maps	p-value	FDR
1	Neurophysiological process_ACM regulation of nerve impulse	3.104E-04	2.917E-02
2	Neurophysiological process_Kappa-type opioid receptor in transmission of ner	3.409E-03	1.242E-01
3	Nicotine signaling in glutamatergic neurons	4.116E-03	1.242E-01
4	Keratan sulfate metabolism p.2	5.715E-03	1.242E-01
5	Apoptosis and survival_Apoptotic TNF-family pathways	6.604E-03	1.242E-01
6	Ascorbate metabolism	5.149E-02	1.867E-01
7	Cytoskeleton remodeling_Alpha-1A adrenergic receptor-dependent inhibition c	5.428E-02	1.867E-01
8	Neurophysiological process_Olfactory transduction	5.706E-02	1.867E-01
9	Role of ZNF202 in regulation of expression of genes involved in atherosclerosi	5.982E-02	1.867E-01
10	Taurine and hypotaurine metabolism	6.259E-02	1.867E-01
Enrichment by GO Localizations			
#	Localizations	p-value	FDR
1	plasma membrane	7.270E-08	9.160E-06
2	integral to membrane	3.243E-06	2.043E-04
3	membrane	2.516E-05	1.057E-03
4	collagen	6.476E-05	2.040E-03
5	integral to plasma membrane	1.394E-04	3.514E-03
6	voltage-gated calcium channel complex	2.292E-04	4.813E-03
7	dendrite terminus	5.940E-04	1.069E-02
8	proteinaceous extracellular matrix	2.719E-03	4.283E-02
9	postsynaptic density	3.718E-03	4.329E-02
10	collagen type XIII	4.123E-03	4.329E-02

Geminin expression co-correlated genes in medulloblastoma

probeset	HUGO	R-value	R-pvalue	probeset	HUGO	R-value	R-pvalue	probeset	HUGO	R-value	R-pvalue	probeset	HUGO	R-value	R-pvalue	probeset	HUGO	R-value	R-pvalue
2898597	GMNN	0.629	1.38E-23	247074	PSNAs	0.638	5.01E-11	3042421	HNRNP2A8	0.586	4.95E-09	2540578	E2F8	0.588	8.72E-08	3592366	SPATA1	0.52	5.64E-07
294777	TKF	0.829	1.86E-23	230273	KRC2C	0.638	5.01E-11	226326	HSPA10	0.585	4.95E-09	2407349	SP3A3	0.547	9.17E-08	2533765	ITGB1BP1	0.519	5.97E-07
2980241	FBX05	0.829	1.87E-23	2858688	ERC8C	0.637	5.07E-11	2396480	EXOSC10	0.585	5.53E-09	2464489	HNRNP1U	0.547	9.05E-08	2828812	MRRP30	0.519	5.85E-07
2894663	PAK1IP1	0.779	1.22E-19	2679796	THOCT7	0.636	3.36E-11	2616018	CNOT10	0.584	5.83E-09	2967650	RTNAP10	0.547	9.04E-08	2981816	PHIP	0.519	5.81E-07
2451200	UBE2T	0.779	1.22E-19	2805786	TARS	0.636	3.36E-11	3129149	PBK	0.584	5.62E-09	3011977	GTBP10	0.547	9.98E-08	2964200	UBE2J1	0.519	5.91E-07
2813442	CENPH	0.771	4.40E-18	2811745	POI11	0.636	3.04E-11	3290210	ZWINT	0.584	5.78E-09	3020804	NAA38	0.547	9.41E-08	3176999	RM1	0.519	5.99E-07
3776138	NDC80	0.761	2.20E-17	3009143	MRRP517	0.636	3.16E-11	2940987	SLC35B3	0.583	6.12E-09	2750594	MSMO1	0.546	9.63E-08	3456262	RPAP3	0.519	5.85E-07
2793951	HMG82	0.758	3.08E-17	2746289	LSM6	0.635	6.52E-11	3458133	PRM1	0.581	7.21E-09	3421177	NUIP107	0.546	9.91E-08	2515749	RBMA5	0.518	6.24E-07
2411228	STIL	0.755	4.66E-17	3291435	RTKN2	0.635	6.60E-11	2469252	RRM2	0.58	8.18E-09	3781429	RRBP8	0.546	9.82E-08	2821273	PPWD1	0.518	6.24E-07
2494484	NCAPH	0.755	4.87E-17	2380554	RRP15	0.634	7.33E-11	2689208	NA50	0.58	7.77E-09	2434490	ENSA	0.545	1.03E-07	2982979	CDYL	0.518	6.25E-07
2416218	ITGB3BP	0.752	6.37E-17	2740005	LARP7	0.634	7.61E-11	2709062	TRA2B	0.58	7.79E-09	2512601	TANK	0.545	1.08E-07	2998404	RALA	0.518	6.36E-07
2973168	ECHDC1	0.751	7.08E-17	2491335	PTDC3	0.632	9.30E-11	2745220	ZNF330	0.579	8.80E-09	2609560	THUMPD3	0.545	1.03E-07	3262165	TAF5	0.518	6.33E-07
2929306	LTV1	0.75	8.40E-17	3881443	TPX2	0.632	9.09E-11	2860666	TAF9	0.579	8.57E-09	2773007	SDA1	0.545	1.05E-07	3482888	GT3A	0.518	6.24E-07
2780172	GENPE	0.747	1.37E-16	2553970	PNP1T	0.631	9.90E-11	3269662	BCIP1	0.579	8.60E-09	2902736	C6orf48	0.545	1.04E-07	3799542	CEP76	0.518	6.23E-07
2364438	NUF2	0.741	3.27E-16	2943809	WTAP	0.63	1.13E-10	2401275	HNRNPR	0.578	9.80E-09	3312490	MK167	0.545	1.03E-07	2386397	GGPS1	0.517	6.67E-07
2388219	EXO1	0.734	1.03E-15	3342426	C11orf82	0.629	1.22E-10	3591704	WDR76	0.577	1.02E-08	2549455	THUMPD2	0.544	1.12E-07	3388914	OCUN105	0.517	6.69E-07
2748163	MND1	0.731	1.44E-15	4012142	ERCC6L	0.627	1.57E-10	2333136	CDC20	0.576	1.16E-08	2495782	LPT1	0.543	1.21E-07	3567469	TRMT5	0.517	6.57E-07
2783715	MAD2L1	0.73	1.52E-15	2818454	KRCC4	0.626	1.58E-10	3082181	NCAPG2	0.576	1.09E-08	2519756	WDR75	0.543	1.26E-07	3804000	INOB80	0.517	6.74E-07
2813414	CCNB1	0.729	1.84E-15	3938913	CDC45	0.626	1.62E-10	2363902	DUSP12	0.575	1.20E-08	2491702	USP39	0.542	1.28E-07	3884882	FAM83D	0.517	6.62E-07
2921374	RFP2	0.728	1.91E-15	2730351	UTP3	0.625	1.83E-10	2523144	NOF98	0.575	1.24E-08	2920862	FIG4	0.542	1.36E-07	3956433	CHEK2	0.517	6.66E-07
2377896	MCMB6	0.728	2.85E-15	2815455	UTP15	0.623	2.12E-10	2610241	KIF20B	0.575	1.39E-08	3412008	UTP18	0.542	1.31E-07	3352388	MAN1A2	0.516	7.17E-07
2488923	SPF3	0.722	4.01E-15	2353733	ITTF2	0.622	2.31E-10	3235389	MCAM10	0.575	1.35E-08	2511189	MTRF1	0.546	1.31E-07	2422885	GLMN	0.516	6.98E-07
2742985	PLK4	0.721	5.17E-15	2445118	METTL8	0.622	2.45E-10	3779684	PSMG2	0.575	1.19E-08	3840142	ZNF480	0.542	1.35E-07	2478017	MORF2	0.515	7.75E-07
2852875	ECT2	0.717	5.86E-15	2858992	DEPDC1B	0.622	2.32E-10	2547716	FAM98A	0.574	1.29E-08	2385197	GNPAT	0.541	1.44E-07	2517408	AGPS	0.515	7.47E-07
2951300	TAF11	0.712	5.49E-15	2948564	MDC1	0.622	2.33E-10	2548871	HNRPL	0.574	1.33E-08	2892738	PRPF4B	0.541	1.43E-07	2845274	CDC127	0.515	7.77E-07
2739864	PRR11	0.711	5.85E-15	2957126	MCM3	0.622	2.34E-10	2862716	GM2	0.574	1.32E-08	2984573	SFT2D1	0.541	1.38E-07	2858484	MCCS2	0.515	7.47E-07
2908572	CDCL5	0.717	6.61E-15	2954678	XPO5	0.621	2.58E-10	2915491	CYB5R4	0.574	1.26E-08	2465519	ZNF689	0.54	1.53E-07	3004768	ZNF273	0.515	7.42E-07
2425447	DPH5	0.716	6.77E-15	3005069	ZNF92	0.621	2.68E-10	2841528	BNP1	0.573	1.38E-08	2483016	CDC104	0.54	1.48E-07	3197528	PLGRKT	0.515	7.52E-07
3959793	CCNB2	0.715	1.06E-14	3539147	SNAPC1	0.62	2.97E-10	2902559	CSNK2B	0.573	1.38E-08	2485176	MDH1	0.54	1.53E-07	3624362	LEO1	0.515	7.43E-07
2604254	HUWRP	0.713	1.35E-14	2746024	ABCE1	0.619	3.03E-10	3090697	CDC42	0.573	1.35E-08	2869275	GIN1	0.54	1.51E-07	4002809	APOO	0.515	7.63E-07
2522212	SGOL2	0.711	1.72E-14	2971378	GOPC	0.619	3.03E-10	3788049	SKA1	0.573	1.40E-08	2967321	PREP	0.54	1.47E-07	2452319	RRBP5	0.514	8.37E-07
2570616	BUB1	0.711	1.78E-14	2980812	TFB1M	0.619	3.04E-10	2728224	SRP72	0.572	1.50E-08	2773655	ROHY1	0.539	1.55E-07	2486520	ETAA1	0.514	8.76E-07
3011454	DBF4	0.709	2.03E-14	2916390	ORC3	0.618	3.21E-10	2738723	HADH	0.572	1.46E-08	2972759	HDDC2	0.539	1.59E-07	2678864	PSMD6	0.514	8.31E-07
2665574	SDF1	0.707	2.68E-14	2940005	MRRP510	0.618	3.26E-10	2823820	WDR36	0.572	1.55E-08	2734956	TIMM17A	0.538	1.75E-07	3345593	CEP57	0.514	7.95E-07
2752725	NEL3	0.704	3.97E-14	3019401	ZNF277	0.618	3.23E-10	2339414	USP1	0.571	1.64E-08	2454532	INTS7	0.538	1.79E-07	2529782	MRPL44	0.513	8.72E-07
2966232	COQ3	0.703	4.75E-14	3200611	HAI5B	0.616	3.24E-10	2412988	SELRC1	0.571	1.63E-08	2871717	CDC112	0.538	1.78E-07	2834093	TCEG1	0.513	8.68E-07
2919873	ORSL1	0.7	7.25E-14	3433747	RFC5	0.618	3.21E-10	3097152	MCM4	0.571	1.55E-08	2913983	SENP6	0.538	1.69E-07	2975287	HSB1L	0.513	8.42E-07
3658925	ORC6	0.7	6.74E-14	2583352	GTFC3C3	0.617	3.65E-10	2917762	MANEA	0.57	1.77E-08	2766359	RFC1	0.537	1.89E-07	2991103	BZW2	0.513	8.89E-07
2908100	POLH	0.699	7.79E-14	2923599	ASF1A	0.617	3.73E-10	2574884	WIS1	0.569	1.96E-08	2962998	KIAA1009	0.537	1.86E-07	3839142	ZNF473	0.513	8.50E-07
2983721	RIOK1	0.696	1.19E-13	3273338	KIF20B	0.615	4.44E-10	2653902	PNP39	0.569	1.98E-08	3396736	PUS3	0.537	1.92E-07	3592380	BDJ13	0.512	8.97E-07
2411288	DEPDC1	0.695	1.29E-13	2985466	PTTG1	0.614	4.84E-10	3046428	ZNF107	0.569	2.02E-08	3339859	MRP18	0.537	1.86E-07	4012945	ABO37	0.512	9.11E-07
2951674	SRPK1	0.695	1.27E-13	3367338	KIF18A	0.614	4.84E-10	3716893	ATAD5	0.569	1.83E-08	3339862	ALG6	0.536	2.02E-07	2406768	MRRP515	0.512	9.11E-07
3331903	FAM111B	0.694	1.34E-13	3590388	NUSAP1	0.612	6.06E-10	2402068	SYT2	0.568	1.97E-08	2584535	PP1L3	0.536	2.02E-07	2541164	CZMH4	0.511	9.91E-07
2481142	MSH6	0.693	1.54E-13	3775842	TYMS	0.611	6.26E-10	2523439	BZWI	0.568	2.08E-08	2712906	RNF168	0.536	2.03E-07	2978786	PP1L4	0.511	9.51E-07
2958670	RAB23	0.691	1.90E-13	3629874	LUMPS	0.61	6.78E-10	2853768	NUP155	0.568	2.03E-08	2839671	RARS	0.536	2.00E-07	3343008	TMEM126A	0.511	9.66E-07
2450345	KIF14	0.689	2.26E-13	2847710	FASTKD3	0.61	6.74E-10	3073597	CHCHD3	0.568	1.97E-08	2918246	SMIM8	0.536	2.03E-07	3869461	ZNF616	0.511	9.86E-07
2458742	LIN9	0.689	2.32E-13	2744955	TACC3	0.609	7.52E-10	2406420	CLSPN	0.567	2.17E-08	2940551	SSR1	0.536	2.00E-07	4021508	ZNF280C	0.511	9.66E-07
3603408	PSMA4	0.688	2.62E-13	3795888	TMM21	0.609	7.58E-10	3474495	TRAP1	0.567	2.13E-08	3821908	RNASEH2A	0.536	1.96E-07	2412529	NRD1	0.51	1.03E-06
2346399	CDC7	0.686	3.70E-13	2704188	PCDD10	0.608	7.97E-10	2407191	GNL2	0.566	2.37E-08	2404377	SNRNP40	0.536	2.10E-07	2476411	TTCT2	0.51	1.03E-06
2412799	ORC1	0.685	4.11E-13	3468261	NUP37	0.608	7.96E-10	2775858	LIN5A	0.566	2.43E-08	2406245	PSMB2	0.535	2.15E-07	2828856	HSPA4	0.51	1.